中正嶺學報 第三十三卷 第二期 民國 94.5.
JOURNAL OF C.C.I.T., VOL.33, NO.2, MAY, 2005

Mixed Convection in an Isothermally Horizontal Channel with Packed Spheres

Pai-Yu Chang and Sheau-Wen Shiah

Department of Naval Architectur and Marine Engineering
Chung Cheng Institute of Technology
National Defense University

ABSTRACT

This study ignores the nonlinear inertia terms of non-Darcian mixed convection in an isothermally horizontal channel with packed spheres (stainless sphere and water). The important characteristics of non-Darcian convection are the no-slip boundary, flow inertia, channeling effect and thermal dispersion effect. The ranges of the Rayleigh number Ra= $0\sim 2\times 10^5$, and the Peclet number Pe= 10~300 are used in this study. A secondary flow, induced by the buoyancy effect, occurs when Ra is high and Pe is low. However, as Pe increasing, the buoyancy effect is suppressed because thermal dispersion effect dominates.

Key words: non-Darcian, secondary flow, buoyancy effect, thermal dispersion effect

等溫水平矩形填充球管內之混合熱對流

張百禹　夏曉文

國防大學中正理工學院造船工程學系

摘　　要

本文研究在忽略非達西理論之非線性慣量項，於等溫之水平矩形填充（不銹鋼珠及水）管內混合熱對流之數值模擬；非達西理論包括無滑動邊界、流動慣量、槽道效應及熱分散效應。其中雷利數計算範圍 Ra = $0\sim 2\times 10^5$，而沛克雷數計算範圍 Pe = 10~300，當高雷利數及低沛克雷數時，管內受溫度差導致浮力效應進而引發二次流結果。但是，當沛克雷數逐漸增加時，熱分散效應明顯主導了整個熱傳結果，並且抑制了浮力效應。

關鍵詞：非達西，二次流，浮力效應，熱分散效應

文稿收件日期 93.6.4; 文稿修正後接受日期 93.8.30.
Manuscript received June 4, 2004; revised Aug. 30, 2004.

I. INTRODUCTION

This study investigates fluid flow and heat transfer in porous media, which have been the subjects of many recent works, as the understanding of associated transport processes in various engineering systems has become increasingly important. Such systems include, for example, packed-sphere beds, solid matrix exchangers, and fixed-bed heat-storage systems. Previous studies on convective heat transfer in porous media addressed mostly natural convection or forced convection. Studies of mixed convection are rather few. Wooding [1] and Sutton [2] attempted early on to theoretically determine the conditions that lead to mixed convection. The study of Combarnous and Bia [3] was one of the first to apply experiments and numerical computation to the effect of mean flow on the onset of convection in a porous medium bounded by isothermal planes. Cheng [4] and Minkowycz et al. [5] conducted a series of studies on mixed convection over vertical, inclined and horizontal plates in porous media. Haajizadeh and Tien [6] investigated mixed convective flow through a horizontal porous channel that connected two reservoirs.

All of the aforementioned theoretical studies adopted Darcy's law to formulate the problems. However, Darcy’s law only applies to low-velocity, small-pore, or low-permeability porous medium systems, so high-velocity and large-pore medium systems require the use of a non-Darcian law. Recently, Angirasa and Peterson [7] used highly porous thin fibrous materials with a high Reynolds number in a channel, and isothermally heated the walls in a localized region, to simulate the effects of an electronic component. Chandrasekhara and Namboodiri [8] used a non-Darcian model that included the variations of permeability and thermal conductivity to study mixed convection over inclined surfaces and found that these variations significantly affected heat transfer. Lai and Kulacki [9] used the similarity method and a non-Darcian model that incorporates the inertial effect to study mixed convection over horizontal plates in a porous medium. Alazmi and Vafai [10] reported the effects of the Darcian number, the inertia parameter, the Reynolds number, porosity, the diameter of the particles, and the fluid-to-solid conductivity ratio in a parallel plate channel. Chou et al. [11] considered the effect of disregarding the nonlinear inertia terms of non-Darcian mixed convection in the fully developed region of horizontal packed-sphere channels. Chou and Chang [12] showed that the effect of stagnant conductivity can be characterized by the conductivity ratio of a solid-sphere to the fluid, which affects considerably the secondary flow structure and heat transfer rate. Chou and Chang [13] also proved that the errors induced by neglecting the nonlinear inertia terms are all less than 1 % in Nusselt number for the cases of Pr= 100, 10 and 6.5, Pe= 10- 100, and Rayleigh number up to 10^5. Notably, all of the above works pertain to thermally fully developed region.

The thermal boundary conditions on the treated entrance problems have included follows: uniform wall heat flux through the wall in the axial and peripheral directions [14, 15], isothermal ducts [16, 17], or axially uniform

heating and peripherally uniform wall temperature [18]. Literature on the packed-sphere channel in the entrance region is very limited. To the authors' knowledge, no study has disregarded the nonlinear inertia terms of the non-Darcian mixed convection for an isothermally horizontal channel with packed spheres in the thermally developing entrance region.

II. THEORETICAL ANALYSIS

The present analysis uses non-Darcian law and volume-averaged equations. Characteristics of non-Darcian convection are as follows: no-slip boundary, flow inertia, channeling effect, and thermal dispersion effect. In vector notation, the steady state for three-dimensional generalization of continuity, momentum, and energy equations for mixed convection in porous media are written as follows:

$$\nabla \cdot <\hat{V}>=0 \tag{1}$$

$$(\rho/\varepsilon^2)<\hat{V}\cdot\nabla\hat{V}>=-\nabla<P>+\rho\hat{g}-(\bar{\mu}_f/K)<\hat{V}> -\rho C\left|<\hat{V}>\right|<\hat{V}>+(\bar{\mu}_f/\varepsilon)\nabla^2<\hat{V}> \tag{2}$$

$$\rho c_p <\hat{V}>\cdot\nabla<T>=\nabla(k_e\nabla<T>) \tag{3}$$

where < > represents a volume-averaged quantity; $\hat{V}$, P and T are the local velocity vector, pressure, and temperature; ρ and $\bar{\mu}_f$ are the fluid density and viscosity; ε is the porosity; K and C are the permeability and inertial coefficient; and k_e is the effective conductivity. The physical configuration and coordinate system are shown in Fig. 1.

A steady fully developed axial velocity is assumed at the entrance of the heated section; laminar flow in the hydro-dynamically developed

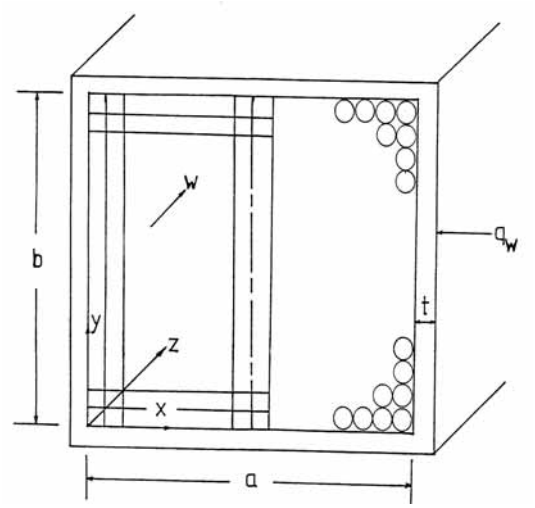

Fig. 1. Physical configuration and coordinate system.

and thermal developing region of packed-sphere horizontal rectangular isothermal channel is studied in this article. Both the viscous dissipation and compressibility effect in the energy equation were disregarded based on the large Prandtl number have low velocity fluids. The large Prandtl number fluids are frequently used in engineering problems, such as water, oil and a lot of chemical solutions. The Boussinesq approximation is used to characterize the buoyancy effect and to discount the nonlinear inertia terms, with the following variables:

$$\begin{aligned} &x=X/d,\quad y=Y/d,\quad \mathrm{z}=\mathrm{Z}/(\mathrm{d}\times Pe),\\ &u=<U>/(\alpha_f/d),\ v=<V>/(\alpha_f/d),\\ &w=<W>/<\overline{W}>,\quad \mathrm{Da}=\mathrm{K}_\infty/\mathrm{d}^2,\\ &\theta=(<T_w>-<T>)/(<T_w>-<T_i>),\\ &\mathrm{Re}=<\overline{W}>d/\overline{\nu}_f,\quad \mathrm{Pr}=\overline{\nu}_f/\alpha_f,\quad Pe=\mathrm{Pr}\,\mathrm{Re},\\ &Ra=g\beta q_w d^4/(\overline{\nu}_f\alpha_f k_f) \end{aligned} \tag{4}$$

and introducing the stream function and vorticity,

$$u=\partial\psi/\partial y,\quad v=-\partial\psi/\partial x \tag{5}$$

$$\xi=\partial u/\partial y-\partial v/\partial x \tag{6}$$

the governing equations can be obtained:

$$\nabla^2\psi = \xi \tag{7}$$

$$\begin{aligned} 0 &= -(\varepsilon d^2/K)\xi + \nabla^2\xi + 300(1-\varepsilon) \\ &(u\partial\varepsilon/\partial y - v\partial\varepsilon/\partial x)/\varepsilon^3 + \varepsilon Ra(\partial\theta/\partial x) \\ &+ Ra\,\theta(\partial\varepsilon/\partial x) \end{aligned} \tag{8}$$

$$\begin{aligned} 0 &= \varepsilon[-K_\infty(dP/dZ)/(\overline{\mu}_f < \overline{W} >)]/Da \\ &-(\varepsilon d^2/K)w - \varepsilon Cd\,\mathrm{Re}\,w^2 + \nabla^2 w \end{aligned} \tag{9}$$

$$\begin{aligned} &u\partial\theta/\partial x + v\partial\theta/\partial y + w\partial\theta/\partial z \\ &= (\partial/\partial x)[(k_e/k_f)(\partial\theta/\partial x)] \\ &+ (\partial/\partial y)[(k_e/k_f)(\partial\theta/\partial y)] \end{aligned} \tag{10}$$

where $\nabla^2 = (\partial^2/\partial x^2 + \partial^2/\partial y^2)$. The Darcian number Da relates the core permeability K_∞ to the diameter of the packed-sphere d; the value of D_e /d is calculated as 10 throughout the present work.

2.1 Calculation of Parameters

From the experimental results of Benenati and Brosilow [19], the porosity, ε , can be represented approximately by a decaying cosine function as mentioned by Hunt and Tien [20]:

$$\varepsilon = \varepsilon_\infty[1 + a_1\exp(-a_2 n/d)\cos(2\pi n/d)] \tag{11}$$

where ε_∞ is the porosity at the core region, *n* is the distance from the wall in the inward normal direction, *d* is the particle diameter, and a_1 and a_2 are empirical coefficients which depend on the packing condition and particle size. The value of ε_∞ = 0.365 was measured in the corresponding experiment [11]. The coefficients a_1 = 0.43 and a_2 = 3 have been experimentally verified by Renken and Poulikakos [21]; therefore, they are also used in the present numerical work. For a liquid-saturated porous medium, the permeability *K* and the flow inertial parameter *C* depend on the matrix porosity and sphere diameter, which are given by the relations developed by Ergun [22]:

$$K = d^2\varepsilon^3/[150(1-\varepsilon)^2] \tag{12}$$

$$C = 1.75(1-\varepsilon)/(d\varepsilon^3) \tag{13}$$

The effective conductivity k_e is composed of a sum of the stagnant and dispersion conductivities, $k_e = k_o + k_d$. The value of stagnant conductivity depends on the porosity variation and the conductivities of the fluid and solid. The variation of stagnant conductivity near the wall can be written as used by Kuo and Tien [23]:

$$k_o = k_\infty[1 + (k_f/k_\infty - 1)\exp(-a_3 n/d)] \tag{14}$$

where a_3 is an empirical constant and k_∞ is the conductivity in the core region, which can be obtained from the semi-theoretical model by Zehner and Schlunder [24]:

$$\begin{aligned} k_\infty &= k_f\{1-(1-\varepsilon_\infty)^{0.5} + 2\Lambda(1-\varepsilon_\infty)^{0.5} \\ &[B_o\Lambda(\Lambda-1)\ln(\Lambda/B_o)/(\Lambda-B_o)^2 - (B_o+1)/2 \\ &-\Lambda(B_o-1)/(\Lambda-B_o)]/(\Lambda-B_o)\} \end{aligned} \tag{15}$$

where $B_o = 1.25[(1-\varepsilon_\infty)/\varepsilon_\infty]^{10/9}$ and $\Lambda = k_s/k_f$.

From Eqs. (14) and (15), one can see that the effect of stagnant conductivity is characterized by the conductivity ratio of solid sphere to fluid, k_s/k_f. The values of thermal conductivities for stainless steel spherical beds, k_s= 16.5 W/m K, and water, k_f= 0.616 W/m K. Therefore, Pr= 10 and $\Lambda = k_s/k_f$ = 26.8 is used for water-stainless steel spherical beds in the present work.

The dispersion conductivity k_d incorporated the additional thermal transport due to the fluid's tortuous path around the solid particles. This quantity is proportional to a product of the local velocity, a constant γ_∞ , and wall function:

$$k_d = k_f\gamma_\infty Pe\{[(u^2+v^2)/Pe^2] + w^2\}^{0.5} l(n)/d \tag{16}$$

where $l(n)$ is the wall function for thermal

dispersion damping near the wall, which is given by Kuo and Tien [23] as

$$l(n) = d\{1 - \exp[-n/(a_4 d)]\} \quad (17)$$

where a_4 is an empirical constant. There are two different sources to show the wall effect on thermal dispersion. First, the no-slip boundary condition and the near-wall porosity variation modify the velocity distribution near the wall. Second, the mixing of a local fluid stream is reduced by the presence of a wall. The value $\gamma_\infty = 0.07$ used by Kuo and Tien [23] from the mixing-length concept and statistical averaging process. Values $a_3 = 1$ and $a_4 = 1$ were verified by comparing theoretical and experimental results of forced and mixed convection [11]. The boundary conditions are:

$$u = v = w = \theta = 0 \quad \text{at the wall} \quad (18a)$$

$$u = \partial v/\partial x = \partial w/\partial x = \partial\theta/\partial x = 0 \quad \text{at } x = \text{a/2} \quad (18b)$$

$$u = v = \xi = \psi = \theta = 0 \quad \text{at z= 0} \quad (18c)$$

By finite difference scheme to obtain the numerical solutions for u, v, w, ξ and θ, and from DuFort-Frankel method [25], the bulk temperature for next axial position θ_b can be solved from Eq. (10). The local Nusselt number Nu_l is evaluated on the basis of the overall energy balance:

$$Nu = -(D_e/d)^2(\partial\theta_b/\partial z)/4\theta_b \quad (19)$$

where subscript b denotes the bulk quantity.

III. RESULTS AND DISCUSSION

To track accurately the near-wall porosity variation and the near-wall damping of dispersion conductivity, a non-uniform grid system ($\Delta x_i = 1.05\Delta x_{i-1}$, $\Delta y_j = 1.05\Delta y_{j-1}$) is used. A numerical experiment was made to ensure the independence of the numerical results on the size $M \times N$ and axial step Δz. Table 1 presents the values of Nu_l calculated by using $M \times N = 50 \times 100$, 40×80 and 36×72 ; $\Delta z_u = 10^{-3}$ and 5×10^{-4} ; $\sigma_1 = 1.01$ and 1.003 at some selected axial positions for the case of Pr= 10, Ra= 10^5, a/b=1, and $\Delta z_1 = 4 \times 10^{-5}$, where σ is a grid ratio constant in the z direction, subscript u denotes the uniform quantity. The deviation of Nu_l for $M \times N$ $(\Delta z_u, \sigma_1) = 40 \times 80(10^{-3}, 1.01)$ and $40 \times 80\,(5 \times 10^{-4}, 1.003)$ is less than 0.45 %, and Nu_l for $40 \times 80(10^{-3}, 1.01)$ and $50 \times 100(10^{-3}, 1.01)$ is less than 1.1%. Therefore the mesh size and axial step size $M \times N\,(\Delta z_u, \sigma_1) = 40 \times 80(10^{-3}, 1.01)$ was used in this article.

Table 1. Numerical results of Nu for the case of D_e/d= 10, Pr=10, Ra=10^5, Pe=10 and $\Delta z_1 = 4 \times 10^{-5}$

$M \times N$ z $(\Delta z_u, \sigma_1)$ Nu	0.0205	0.1006	0.4996
40×80 $(1 \times 10^{-3}, 1.010)$	51.4944	23.2476	17.1672
40×80 $(5 \times 10^{-4}, 1.003)$	51.2624	23.1572	17.1893
50×100 $(1 \times 10^{-3}, 1.010)$	51.6216	23.3247	17.0912
36×72 $(1 \times 10^{-3}, 1.010)$	51.4796	23.2379	17.2114

Figure 2 illustrates the axial velocity profile along the symmetry line x= a/2 of a horizontal isothermal packed channel (a/b= 1 and D_e/d= 10) with working fluid water Pr= 10, Peclet number

Pe= 10, 100, and pure forced convection Ra= 0. The behavior of velocity distorted was resulted from the higher porosity induced channel effect in the near-wall region. But, no velocity distortion effect observed for the slug flow by attaching the constant axial velocity, which does not consider the channel effect. Figure 3 further displays the bulk temperature θ_b versus the thermal entrance region *z*, which have the same parameter conditions as in Fig. 2. The forced-flow thermal development effect causes a monotonic decrease of θ_b near the entrance; here, the slug flow has larger velocity, larger momentum in the near-wall, and larger θ_b value in a packed sphere isothermal channel. Moreover, the higher value Pe= 100 induced higher thermal dispersion effect, and has lower bulk temperature θ_b than the value Pe= 10. When z approaches 10, 20 and 30, $\theta_b = 0$ can obtained, respectively, for Pe= 100, 10, and slug flow; for $\theta_b = 0$, it is prescribed that anywhere have the same wall temperature in a packed sphere isothermal channel. Therefore, Pe= 100 has the stronger dispersion effect than Pe= 10 and slug flow, and can easily obtain the bulk temperature $\theta_b = 0$ in a packed sphere isothermal channel.

Following the above conditions of Figs. 2~3, the variation of Nu_l in the thermal entrance region of horizontal isothermal packed channel is shown in Fig. 4. Similarly, a monotonic reduction of Nu_l near the entrance is caused by the forced-flow thermal development effect; when z approaches 10, 20 and 30, obtained the thermal fully developed. The value of Nu_l approaches 18, 9 and 6, respectively for Pe= 100, 10, and slug flow. Moreover, Pe= 100 owing to the higher dispersion effect and has higher Nu_l than Pe= 10 and slug flow have. The slug flow has lower Nu_l values despite having higher θ_b values.

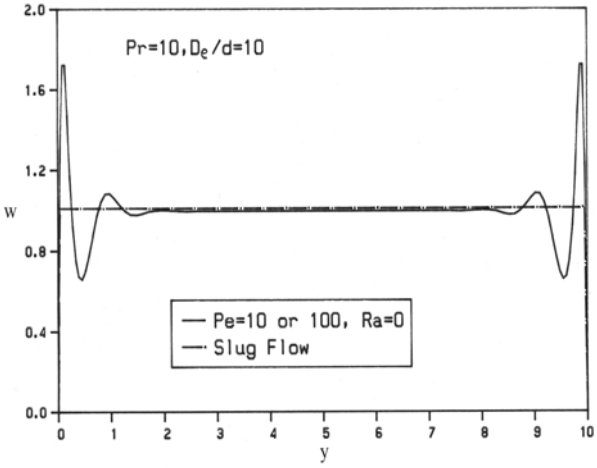

Fig. 2. Axial velocity w along the symmetry line x= a/2 for Ra= 0, Pr= 10, Pe= 10, 100 and slug flow.

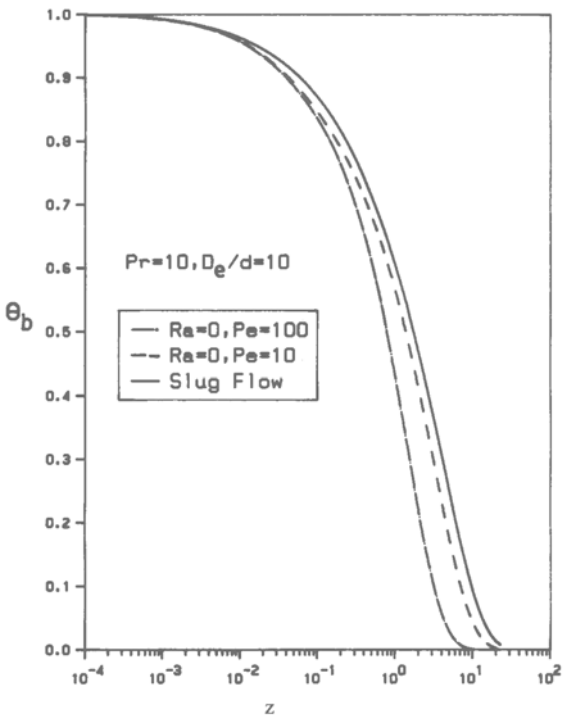

Fig. 3. Bulk temperature θ_b versus z for Ra= 0, Pr= 10, Pe= 10, 100 and slug flow.

Figure 5 shows the variation of Nu_l in the thermal entrance region of the packed sphere isothermal horizontal channel (a/b= 1) with Rayleigh numbers Ra= 0- 5×10^3 , 5×10^4 , 1×10^5 and 2×10^5 , for Pe= 10, and Pr= 10. A monotonic decrease of Nu_l near the entrance is caused by the forced-flow thermal development effect. The onset of the buoyancy effect occurs at a specified distance from the entrance, which depends primarily on the value of the Ra, with higher Ra inducing a stronger buoyancy effect. However, the buoyancy effect is negligible for certain regions of the lower Ra (for example, $0-5\times10^3$). The other curves of Nu_l deviate from the curve for Ra= $0-5\times10^3$ owing to heat transfer enhancement resulting from the development of the secondary flow induced by the buoyancy effect. Clearly, Nu_l will not be minimized unless the entrance effect balances the buoyancy effect, and each curve ultimately approaches an asymptotic value when the temperature profile is fixed in the fully developed region. To understand the instability phenomenon of secondary flow induced by the buoyancy effect, Nakayama et al. [26] employed an analytic method of linear instability to clarify the position of axial roll for the parallel plate. Incropera et al. [27] also predicted the position of secondary flow at the thermal entrance and the combined entrance region, and their results reveal one order of error with the experimental data. Although many studies exist on the instability phenomenon of secondary flow under axially uniform heating, the author is now aware of a steady model having previously been used. A stronger disturbance phenomenon occurs when the Rayleigh number Ra is 2×10^5. Clearly, a minimum Nu_l will not appear unless the buoyancy effect is balanced by the stronger forced convection induced thermal dispersion effect. When the fully developed region is reached at about z= 10, all of the curves reach the same local minimum in the isothermal channel. And from the step z= 10, the bulk temperature approaches the wall temperature, and the buoyancy effect is completely suppressed.

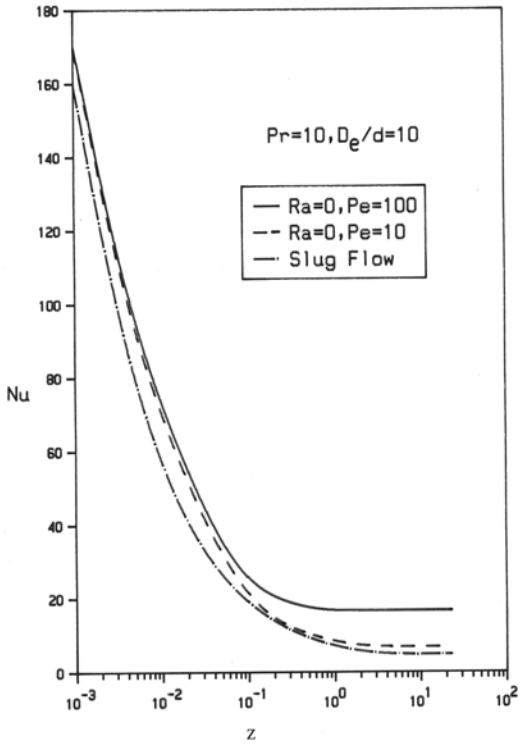

Fig. 4. Nusselt number Nu versus z for for Ra= 0, Pr= 10, Pe= 10, 100 and slug flow.

Figure 6 shows streamline and isotherm patterns for Ra= 1×10^5, and Pe= 10 as for the curve in Fig. 5. At the onset of the buoyancy effect, z= 0.1996 (Fig. 6a). Fluid is heated near the wall, the buoyancy effect induces an upward flow near the left wall and a downward flow near the center of the channel, resulting in a single

eddy. At this time, the isotherm near the bottom horizontal heated wall remains unaffected by the buoyancy effect. At z= 0.8396 (Fig. 6b), the streamline and isotherm become more irregular than z= 0.1996. At z= 0.8396 has stronger secondary flow, higher heat transfer rate, the first peak of Nu_l forms; moreover, an adverse temperature gradient forms near the bottom heated wall, and induces smaller eddy than the counter-rotation eddy due to temperature accumulation near the left corner of the bottom heated wall. Thereafter, the temperature gradient and the effect of buoyancy decrease toward the point z= 10 (Fig. 6c), the buoyancy effect gradually decreases as the asymptotic temperature is approached. When the bulk temperature approaches the wall temperature, attaches only an eddy reappears.

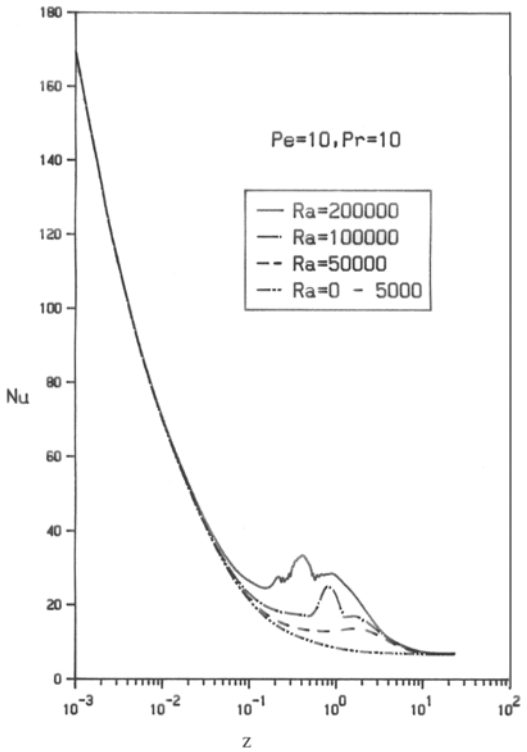

Fig. 5. Nusselt number Nu versus z for Pr= 10, Pe= 10 and various Ra.

(a) z= 0.1996

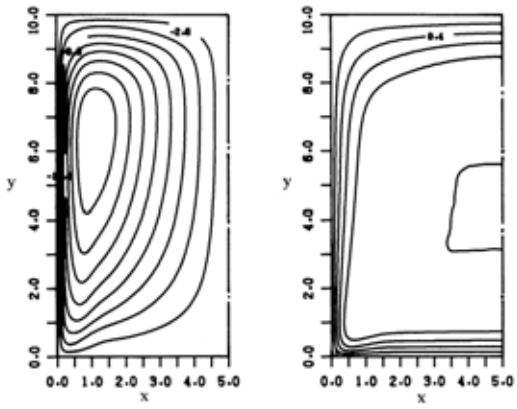

(b) z= 0.8396

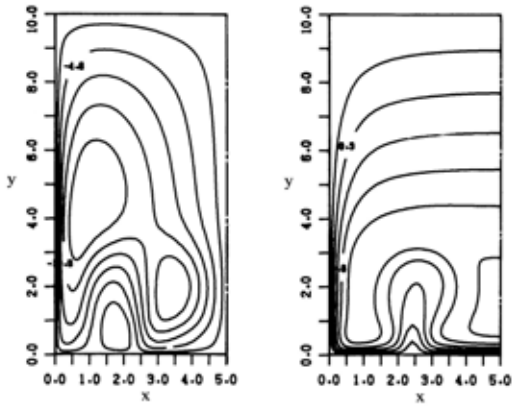

(c) z= 10

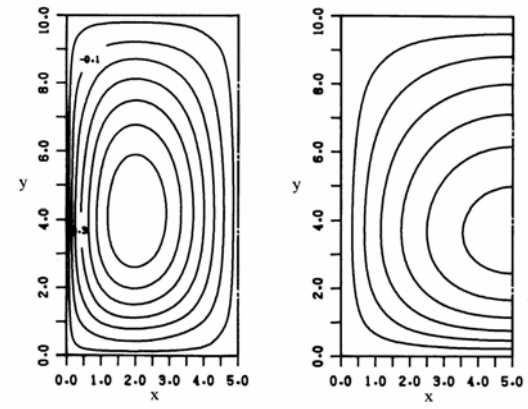

Fig. 6. Streamlines and isotherms for Pe= 10, Pr= 10, Ra= 1×10^5 and various axial direction in (a) z= 0.1996 (b) z= 0.8396 (c) z= 10.

Besides the buoyancy effect induced by Ra, the thermal dispersion effect induced by Pe is also extremely important. Figure 7 shows the effect of thermal dispersion, at Ra= 1×10^5, Pr= 10, D_e/d= 10 and Pe= 10, 100, 200 and 300. When Pe= 10, Nu_l is 7.45 in the fully developed region, the curve displays the buoyancy effect along entrance region at z= 0.8396, which the phenomenon of secondary flow is stronger, and the heat transfer rate is higher than other regions. When Pe= 300, Nu_l is 32.37 in the fully developed region, and Pe= 10, Nu_l is 8 in the fully developed region. But, the phenomenon of secondary flow for Pe= 300 is weaker owing to the higher Pe induced thermal dispersion effect, and the buoyancy effect is completely suppressed.

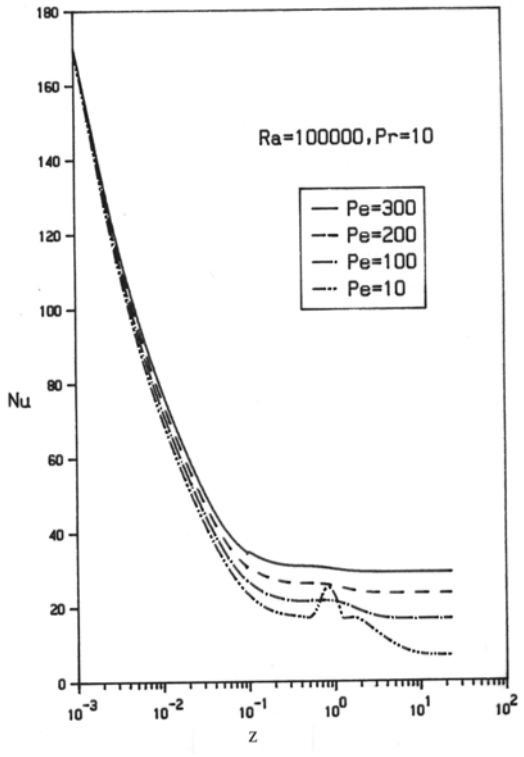

Fig. 7. Nusselt number Nu versus z for Pr= 10, Ra= 10^5, and various Pe.

3.1 Concluding Remarks

(1) The present numerical simulation ignores the nonlinear inertia terms for non-Darcian mixed convection in an isothermally horizontal channel with packed spheres. Non-Darcian convection, including the no-slip boundary, flow inertia, channeling effect and thermal dispersion effect had been considered in a theoretical analysis.

(2) The onset of the buoyancy effect occurs at a particular step in the thermally developing entrance region. The step depends on Rayleigh number Ra. The local Nusselt number, Nu_l, will have no minimum unless the buoyancy effect is balanced by the thermal dispersion effect, and each curve of Nu_l finally approaches an asymptotic value in the fully developed region. However, the buoyancy effect is negligible for certain regions of the lower Ra (for example, $0-5\times10^3$).

(3) Like Ra, Peclet number Pe is also a very important parameter. As increasing Pe (at the larger value Pe= 300 for Ra= 10^5 and Pr= 10), the thermal dispersion effect is induced and the buoyancy effect is also suppressed.

REFERENCES

[1] Wooding, R. A., “Convection in Saturated Porous Medium at Large Rayleigh Number and Peclet Number,” J. Fluid Mech., Vol. 15, No. 4, pp. 527-544, 1963.

[2] Sutton, F. M., “Onset of Convection in a Porous Channel with Net through Flow,” Physics Fluid, Vol. 13, No. 8, pp. 1931-1934, 1970.

[3] Combarnous, M. A. and Bia, P., “Combined Free and Forced Convection in Porous Medium,” Soc. Petrol. Eng. J., Vol. 11, No. 7, pp. 399-405, 1976.

[4] Cheng, P., “Combined Free and Forced Boundary Layer Flows about Inclined Surface in Saturated Porous Media,” Int. J. Heat Mass Transfer, Vol. 20, No. 5, pp. 806-814, 1977.

[5] Minkowycz, W. J., Cheng, P. and Hirschberg, R. N., “Non-Similar Boundary Layer Analysis of Mixed Convection about a Horizontal Heated Surface in a Fluid-Saturated Porous Medium,” Int. Comm. Heat Mass Transfer, Vol. 11, No. 1, pp. 127-141, 1984.

[6] Haajizadeh, M. and Tien, C. L., “Combined Nature and Forced Convection in a Horizontal Porous Channel,” Int. J. Heat Mass Transfer, Vol. 27, No. 6, pp. 799-813, 1984.

[7] Angirasa, D. and Peterson, G. P., “Forced Convection Heat Transfer Augmentation in a Channel with a Localized Heat Source Using Fibrous Material,” ASME J. Electronic Packaging, Vol. 121, No. 1, pp. 1-7, 1999.

[8] Chandrasekhara B. C. and Namboodiri, P. M. S., “Influence of Variable Permeability on Combined Free and Forced Convection about Inclined Surface in Porous Media,” Int. J. Heat Mass Transfer, Vol. 28, No. 1, pp. 199-206, 1985.

[9] Lai, F. C. and Kulacki, F. A., “Non-Darcy Convection from Horizontal Impermeable Surface in Saturated Porous Media,” Int. J. Heat Mass Transfer Vol. 30, No. 10, pp. 2189-2192, 1987.

[10] Alazmi, B. and Vafai, K., “Analysis of Variants within the Porous Media Transport Models,” ASME J. Heat Transfer, Vol. 122, No. 2, pp. 303-326, 2000.

[11] Chou, F. C., Chang, P. Y. and Cheng, C. J., “Effects of Stagnant and Dispersion Conductivities on Non-Darcian Forced Convection in Square Packed-Sphere Channels,” Can. J. Chem. Eng., Vol. 69, No. 6, pp. 1401-1407, 1991.

[12] Chou, F. C. and Chang P. Y., “Effect of Stagnant Conductivity on Non-Darcian Mixed Convection in the Horizontal Square Packed-Sphere Channels,” Numerical Heat Transfer, Part A, Vol. 27, No. 2, pp. 195-209, 1995.

[13] Chou, F. C. and Chang P. Y., “On the Effects of Neglecting the Nonlinear Inertia Terms in the Simulation of on Non-Darcian Mixed Convection in the Horizontal Packed-Sphere Channels,” J. of CSME, Vol. 12, No. 6, pp. 571-579, 1991.

[14] Chou, F. C. and Hwang, G. J., “Vorticity-Velocity Method for Graetz Problem with the Effect of Natural Convection in a Horizontal Rectangular Channel with Uniform Wall Heat Flux,” ASME J. Heat Transfer, Vol. 109, No. 3, pp. 704-710, 1987.

[15] Incropera, F. P. and Schuut, J. A., “Numerical Simulation of Laminar Mixed Convection in the Thermal Entrance Region of Horizontal Rectangular Ducts,” Numerical Heat Transfer, Vol. 8, No. 6, pp.

707-729, 1985.

[16] Hishida, M., Nagano, Y. and Montesclaros, M. S., "Combined Forced and Free Convection in the Entrance Region of an Isothermally Heated Horizontal Pipe," ASME J. Heat Transfer, Vol. 104, No. 1, pp. 153-159, 1982.

[17] Khanafer, K. and Vafai, K., "Isothermal Surface Production and Regulation for High Heat Flux Applications Utilizing Porous Inserts," Int. J. Heat Mass Transfer, Vol. 44, No. 14, pp. 2933-2947, 2001.

[18] Chang, P. Y., Shiah, S. W. and Fu, M. N., "Mixed Convection in a Horizontal Square Packed-Sphere Channel Under Axially Uniform Heating and Peripherally Uniform Wall Temperature," Numerical Heat Transfer: Part A, Vol. 46, No. 2, 2004.

[19] Benenati, R. F. and Brosilow, C. B., "Void Fraction Distribution in Packed Beds," AICHE J., Vol. 8, pp. 359-361, 1962.

[20] Hunt, M. L. and Tien, C. L., "Non-Darcian Convection in Cylindrical Packed Beds," ASME J. Heat Transfer, Vol. 110, No. 2, pp. 378-384, 1988.

[21] Renken, K. J. and Poulikakos, D., "Mixed Convection Experiments about a Horizontal Isothermal Surface Embedded in a Water-Saturated Packed Bed of Spheres," Int. J. Heat Mass Transfer, Vol. 33, No. 7, pp. 1370-1373, 1990.

[22] Ergun, S., "Fluid Flow through Packed Columns," Chem. Eng. Progr., Vol. 48, No. 1, pp. 89-94, 1952.

[23] Kuo, S. M. and Tien, C. L., "Transverse Dispersion in Packed-Sphere Beds," Proc. of the 1988 National Heat Transfer Conf., Houston, pp. 629-634, 1988.

[24] Zehner, P. and Schlunder, E. U., "Thermal Conductivity of Packed Beds at Moderate Temperatures," Chem. Eng. Sci., Vol. 42, No. 5, pp. 933-940, 1970.

[25] Anderson, D. A., Tannehill, J. C. and Pletcher, R. H., Computational Fluid Mechanics and Heat Transfer, McGraw-Hill, New York, 1984.

[26] Nakayama, W., Hwang, G. J. and Cheng, K. C., "Thermal Instability in Plane Poiseuille Flow," ASME J. Heat Transfer, Vol. 92, No. 1, pp. 61-68, 1970.

[27] Incropera, F. K., Knox, A. L. and Schutt, J. A., "Onset of Thermally Driven Secondary Flow in Horizontal Rectangular Ducts," Proc. of 8th Int. Heat Transfer Conf., pp. 1835-1944, 1986.

NOMENCLATURE

A	cross-sectional area of a duct
a	width of rectangular channel
a_1, a_2	coefficients
a_3	stagnant conductivity damping constant
a_4	thermal dispersion damping constant
b	height of rectangular channel
B_o	function defined by equation (15)
C	inertial coefficient, $1.75(1-\varepsilon)/(d\,\varepsilon^3)$
c_p	specific heat at constant pressure
d	particle diameter
Da	Darcian number, K_∞ / d^2
D_e	hydraulic diameter, $4A/S$
g	acceleration due to gravity
$\bar{h}$	average heat transfer coefficient
K	permeability, $d^2\varepsilon^3/[150\,(1-\varepsilon)^2]$

k	thermal conductivity
l	mixing length
M, N	number of division in X, Y direction, respectively
Nu_l	local Nusselt number, $\bar{h}D_h / k_f$
n	inward normal direction or distance from the wall, defined by equation (17)
P	pressure
p	dimensionless pressure
Pe	Peclet number, $PrRe$
Pr	Prandtl number, $\bar{\nu}_f / \alpha_f$
q_w	uniform heat flux
Ra	Rayleigh number, $g\beta q_w d^4 / (\bar{\nu}_f \alpha_f k_f)$
Re	Reynolds number, $<\overline{W}> d / \bar{\nu}_f$
S	perimeter of cross section
T	temperature
U, V, W	velocity components in X, Y, Z direction
u, v, w	dimensionless quantity for U, V, W respectively
$\overline{W}$	average velocity in Z direction
$\overline{w}$	dimensionless quantity for $\overline{W}$
X, Y, Z	rectangular coordinates
x, y, z	dimensionless rectangular coordinates

Greek symbols

α	thermal diffusivity
β	coefficient of thermal expansion with temperature
γ_∞	coefficient in dispersion conductivity
ε	porosity
θ	dimensionless temperature
$\bar{\nu}$	kinematics viscosity
ξ	vorticity in the axial direction, $\partial u / \partial y - \partial v / \partial x$
ρ	density
σ	grid ratio constant in the z direction
ψ	stream function

Subscripts

b	bulk
c	characteristic quantity
d	dispersion
e	effective
f	fluid
i	value at the inlet
o	stagnant
s	solid
u	*uniform*
w	wall
∞	at the core region

Superscripts

—	average value or dimension state
^	vector